Received: 10 September 2021 | Revised: 20 November 2021 | Accepted: 20 November 2021

DOI: 10.1111/jace.18267

Journal of the American Ceramic Society

RESEARCH ARTICLE

Frequency dispersion model of the complex permeability of soft ferrites in the microwave frequency range

Antonio Barba-Juan[1,2] | **Andrés Mormeneo-Segarra**[1,2] | **Nuria Vicente**[1,2] | **Juan Carlos Jarque**[1,2] | **Carolina Clausell-Terol**[1,2]

[1] Departamento de Ingeniería Química, Universitat Jaume I, Castellón, Spain

[2] Instituto Universitario de Tecnología Cerámica, Universitat Jaume I, Castellón, Spain

Correspondence
Carolina Clausell-Terol, Departamento de Ingeniería Química, Universitat Jaume I, 12071 Castellón, Spain.
Email: cclausel@uji.es

Abstract

The complex permeability of Cu-doped nickel-zinc polycrystalline ferrites is strongly dependent on microstructure, particularly, on relative density (ϕ) and average grain size (G). In this study, a mathematical model, able to fit the measured magnetic permeability spectra from 10^6 to 10^9 Hz, is proposed and validated for a width range of average grain sizes (3.40–23.15 μm) and relative densities (0.83–0.96). To the authors' knowledge, domain-wall motion and spin rotation contributions to magnetic permeability have been integrated jointly with the microstructure for the first time in the proposed model, highlighting the relative influence of each magnetizing mechanism and microstructure on the magnetic permeability at different angular frequencies.

KEYWORDS

complex magnetic permeability, domain-wall motion, magnetizing mechanism, microstructure, Ni-Zn ferrites, spin rotation

1 | INTRODUCTION

Ferrites are considered nowadays the leading electromagnetic interference absorbers (EMI), due to its good chemical stability, high resistivity, and excellent electromagnetic properties and cost effective. Ferrites used as EMI applications are classified into two generic types: NiZn and MnZn ferrites. The Cu-doped NiZn ferrites are the most widely used because of their large range of applications in the higher MHz angular frequencies, for example, communication components, microwave devices, multilayer chip inductors, energy storage, sensors, etc. Meanwhile, MnZn ferrites, even with high permeability values, are limited to angular frequencies ranged from kHz to MHz.[1–10]

The magnetic properties of ferrites are mainly determined by their chemical composition and microstructure (e.g., grain size, bulk density, porosity, etc), which in turn, depends on the process variables, such as shaping method and sintering cycles (mainly sintering temperature, dwell time, and atmosphere composition).[2,11]

1.1 | Dependence of complex magnetic permeability on angular frequency

When an alternating current (AC) magnetic field (H) of angular frequency (ω) is applied to the material, the magnetic permeability becomes a complex property with a real (μ') and an imaginary part (μ'')

$$\mu(\omega) = \mu'(\omega) - j \cdot \mu''(\omega) \quad (1)$$

where real part represents the material storage capacity of magnetic field whereas imaginary part represents losses

and power dissipation. Magnetic susceptibility must also be defined as a complex property

$$\chi(\omega) = \chi'(\omega) - j \cdot \chi''(\omega) \quad (2)$$

Permeability and susceptibility are related as follows

$$\mu'(\omega) = 1 + \chi'(\omega) \quad (3)$$

$$\mu''(\omega) = \chi''(\omega) \quad (4)$$

Equations (1) to (4) are well established in literature.[2,12–15]

Moreover, in polycrystalline ferrites, two kinds of magnetizing mechanisms contribute to magnetic permeability: spin rotation and domain-wall motion,[4–7,13,16–19] and, usually, the higher the angular frequency of the magnetic field, the lower the influence of the domain-wall motion mechanism.[13,14,16,18] Accordingly, a magnetic susceptibility for domain-wall motion (χ_d) and a magnetic susceptibility for a gyromagnetic spin rotation (χ_s) can be defined, and Equations (3) and (4) can be rewritten as follows:

$$\mu'(\omega) = 1 + \chi'_S(\omega) + \chi'_{\mathrm{DW}}(\omega) \quad (5)$$

$$\mu''(\omega) = \chi''_S(\omega) + \chi''_{\mathrm{DW}}(\omega) \quad (6)$$

The frequency dispersion of Cu-doped Ni-Zn ferrites, in the angular frequency range studied, exhibits curves where real part is described as a relaxation curve while the imaginary part describes a curve passing through a maximum. Literature [4–7,12–14,16–24] reports several physico-mathematical models defining angular frequency functions for $\chi'_S(\omega)$, $\chi'_{DW}(\omega)$, $\chi''_S(\omega)$, and $\chi''_D(\omega)$ in order to calculate and accurately reproduce the frequency dispersion from Equations (5) and (6). One of the most extended model in polycrystalline ferrites was proposed by Nakamura,[13,18] who kept in mind the influence of spin rotation and domain-wall motion mechanisms on magnetic complex susceptibility, considering that the spin rotation component is of relaxation-type and that the domain-wall motion component is of resonance type, both depending on the angular frequency, leading to the following equations:

$$\mu'(\omega) = 1 + \chi'_S(\omega) + \chi'_{\mathrm{DW}}(\omega) = 1 + \frac{K_S \cdot \omega_S^2}{\omega^2 + \omega_S^2} + \frac{K_{\mathrm{DW}} \cdot \omega_{\mathrm{DW}}^2 \cdot \left(\omega_{\mathrm{DW}}^2 - \omega^2\right)}{\left(\omega_{\mathrm{DW}}^2 - \omega^2\right)^2 + \beta^2 \cdot \omega^2} \quad (7)$$

$$\mu''(\omega) = \chi''_S(\omega) + \chi''_{\mathrm{DW}}(\omega) = \frac{K_S \cdot \omega \cdot \omega_S}{\omega^2 + \omega_S^2} + \frac{K_{\mathrm{DW}} \cdot \omega_{\mathrm{DW}}^2 \cdot \beta \cdot \omega}{\left(\omega_{\mathrm{DW}}^2 - \omega^2\right)^2 + \beta^2 \cdot \omega^2} \quad (8)$$

where K_S is the static susceptibility of the spin rotation, K_{DW} is the static susceptibility of the domain-wall motion, ω_S is the resonance frequency of the spin rotation, ω_{DW} is the resonance frequency of the domain-wall motion, and β is the damping factor of the domain-wall motion.

Equations (7) and (8) allow determining the complex magnetic permeability at any angular frequency but for a sample with a specific microstructure. These equations do not take into account the influence of the microstructure on frequency dispersion.

1.2 | Dependence of complex magnetic permeability on microstructure

Literature reports the strong influence of microstructure on complex magnetic permeability. Particularly, average grain size and relative density play an important role in the magnetization process of polycrystalline ferrites: complex magnetic permeability increases with the average grain size and relative density.[2,3,8,9,11,23-37,39]

However, very few models relating magnetic permeability to microstructure have been developed in the past, and all of them have been uniquely tested at a specific constant angular frequency. In this regard, it is worth mentioning the models proposed by Globus,[36] Rikukawa,[38] Johnson and Visser, [25] and Pankert.[40] Authors have tested these models in polycrystalline ferrites and proven that they are not able to predict the influence of average grain size and porosity on magnetic permeability. Hence, models were modified, and the following relationship, derived from Pankert model, was validated with a good accuracy with the experimental imaginary part of complex permeability [2, 11]:

$$\mu''(\omega) = \mu''_S(\omega) \cdot \psi + \mu''_{\mathrm{DW}}(\omega) \cdot \left[\frac{G^2}{b''(\omega) + G^2}\right] \cdot \psi \quad (9)$$

where b'' is defined as follows:

$$b'' = 4 \cdot \pi^2 \cdot d_W^2(\omega) \quad (10)$$

and ψ is defined from relative density (ϕ), which, in turn, is the ratio of the density to the theoretical density, as:

$$\psi = \frac{\frac{\rho_{\mathrm{real}}}{\rho_{\mathrm{theoretical}}} - \frac{\rho_{\mathrm{lim}}}{\rho_{\mathrm{theoretical}}}}{\frac{\rho_{\mathrm{theoretical}}}{\rho_{\mathrm{theoretical}}} - \frac{\rho_{\mathrm{lim}}}{\rho_{\mathrm{theoretical}}}} = \frac{\phi - \phi_{\mathrm{lim}}}{1 - \phi_{\mathrm{lim}}} \quad (11)$$

In Equations (9) and (10), μ_S'' is the imaginary part-complex magnetic permeability spin rotation contribution, μ_{DW}'' is the imaginary part-complex magnetic permeability domain-wall motion contribution, d_W is the domain-wall width, G is the average grain size, and ψ is the densification defined by Equation (11). Densification ψ is an effective concept when comparing systems of different initial porosities,[41] and $\phi_{\lim}$ stands for the relative density below which the value of the magnetic permeability is virtually zero. This experimental value can be estimated by plotting relative density versus magnetic permeability and extrapolating magnetic permeability to zero.[2,11] For the studied polycrystalline ferrite, a $\phi_{\lim}$ value of 0.65 has been reported.[11]

Authors have satisfactorily tested Equation (9) at four specific angular frequencies (10^6, 10^7, 10^8, and 10^9 Hz), determining for each of the angular frequencies studied the experimental values of the parameters μ_S'', μ_{DW}'', b'', and d_W .[11]

1.3 | Joint dependence of complex magnetic permeability on angular frequency and microstructure

Equations (7) and (8) show the influence of angular frequency on magnetic permeability whereas Equation (9) reveals the influence of microstructure at a specific angular frequency. Equations (8) and (9) can be combined to take into consideration simultaneously both angular frequency and microstructure, and since microstructure has the same influence on the real and imaginary parts of complex magnetic permeability,[25,38,40] the following generalized equations are proposed:

$$\mu'(\omega) = 1 + \left[\frac{K_S \cdot \omega_S}{\omega^2 + \omega_S^2}\right] \cdot \psi + \left[\frac{K_{\mathrm{DW}} \cdot \omega_{\mathrm{DW}}^2 \cdot \left(\omega_{\mathrm{DW}}^2 - \omega^2\right)}{\left(\omega_{\mathrm{DW}}^2 - \omega^2\right)^2 + \beta^2 \cdot \omega^2}\right] \cdot \left(\frac{G^2}{b' + G^2}\right) \cdot \psi \tag{12}$$

$$\mu''(\omega) = \left[\frac{K_S \cdot \omega \cdot \omega_S}{\omega^2 + \omega_S^2}\right] \cdot \psi + \left[\frac{K_{\mathrm{DW}} \cdot \omega_{\mathrm{DW}}^2 \cdot \beta \cdot \omega}{\left(\omega_{\mathrm{DW}}^2 - \omega^2\right)^2 + \beta^2 \cdot \omega^2}\right] \cdot \left[\frac{G^2}{b''(\omega) + G^2}\right] \cdot \psi \tag{13}$$

where b' is constant, [40] and b'' follows the Equation (10).

Summarizing, the present paper aims to:

- Test Equations (12) and (13) to verify their ability to predict complex magnetic permeability (both real and imaginary part) in a wide range of sintered microstructures and angular frequencies.
- Quantify the contribution of each magnetism mechanism on the complex magnetic permeability: Spin rotation and domain-wall motion (terms of the Equations (12) and (13) containing K_S and K_{DW} parameters, respectively).
- Determine the spin rotation static susceptibility (K_S), the domain-wall motion static susceptibility (K_{DW}), the resonance frequency of the spin rotation (ω_S), and the resonance frequency of the domain-wall motion (ω_{DW}). All these parameters are intrinsic characteristics of the material, microstructure-independent, and constants at any angular frequency, allowing different materials to be directly compared.

2 | EXPERIMENTAL PROCEDURE

Cu-doped Ni–Zn-polycrystalline-sintered ferrites are prepared as described in previous papers.[42,43] Hereafter, a brief description of experimental procedure is given.

A polycrystalline ferrite, of chemical composition $Cu_{0.12}Ni_{0.23}Zn_{0.65}(Fe_2O_4)$, supplied by Fair-rite Products Corp. was used as starting powder. It consists of spray-dried granules, with an average size of 175 μm, made up of particles with an average size of 1—2 μm and narrow particle-size distribution. Real density value of 5380 kg·m^{-3} was determined by helium pycnometer.

Cylindrical and toroidal test specimens (3-mm thick and 19-mm external diameter; 6-mm internal diameter for the toroidal test specimens) were shaped by uniaxial dry pressing and sintered by the conventional air solid-state method in an electric laboratory furnace.

Six compaction pressures, (50, 75, 200, 150, 200, and 300 MPa) and 10 dwell sintering times (5, 10, 20, 30, 45, 60, 120, 300, 900, and 1800 min) were used to sinter 60 samples at 1100°C covering a wide range of relative densities (0.83–0.96) and average grain sizes (3.40–23.15 μm). Bulk densities of samples were measured according to Archimedes principle. Relative density (ϕ) of each sample was calculated as the ratio between bulk density and real density of the starting powder (5380 kg·m^{-3}), upon which porosity could be calculated as $(1-\phi)$. Scanning electron microscope (FEG-ESEM Quanta 200F) was used to observe the microstructure of ferrite specimens. Through an image analysis software, average grain size (G) was determined from grain size distribution of the thermal-etched surface cross-sectional area for each specimen. Experimental

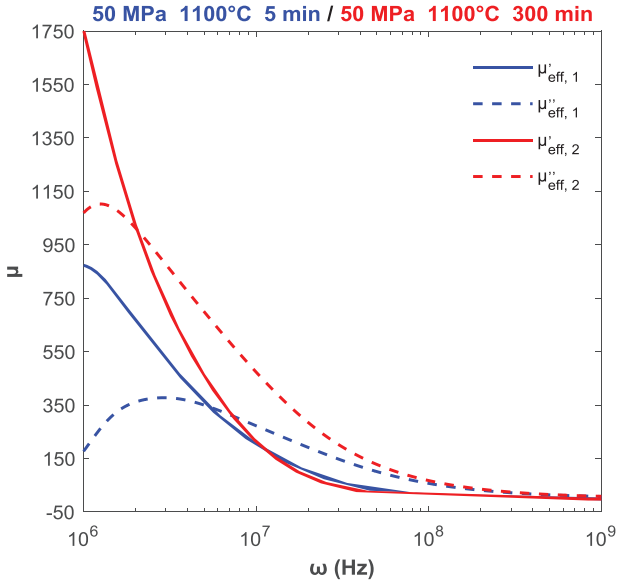

FIGURE 1 Frequency dispersion spectra of complex magnetic permeability (real and imaginary part) of two specimens with different microstructure

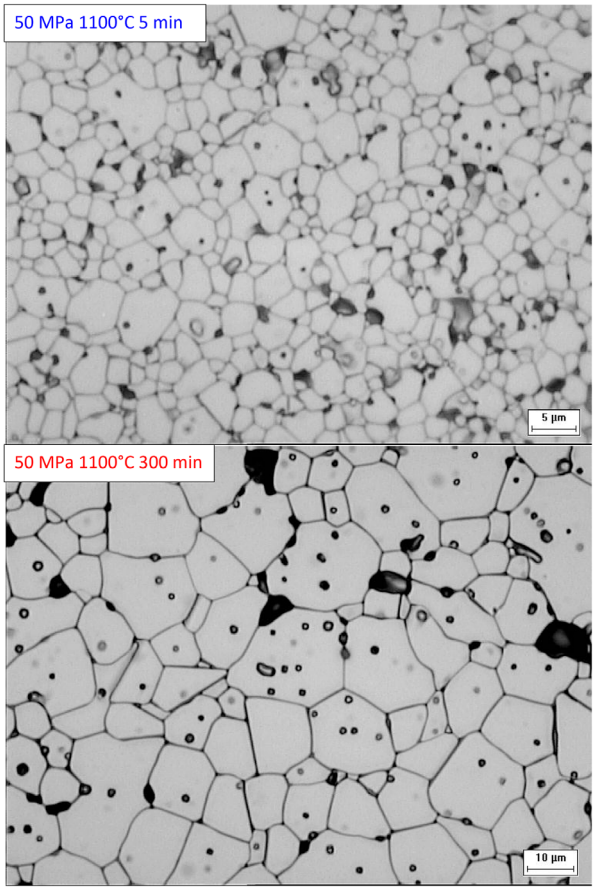

FIGURE 2 Scanning electron micrographs of polished and etched cross-sectional surfaces of both specimens of Figure 1

values of ϕ and G for every specimen are shown in Table 1, together with its absolute error $\varepsilon(\phi)$ and $\varepsilon(G)$. Relative error for ϕ is always lower than 1% whereas the maximum relative error for G is around 10%. Table 1 also shows the amplitude of grain size distribution S as the difference between G_{90} and G_{10}. Grain size distribution is, in all cases, monomodal and relatively narrow, although it becomes wider with increasing both sintering time and temperature.

The complex magnetic permeability (real μ'_{eff} and imaginary μ''_{eff} part) was obtained in an Agilent E4991A RF impedance/material analyser in the 10^6–10^9 Hz frequency range using an Agilent 16454A magnetic material test fixture. Each curve is made up of 800 experimental values in the aforementioned frequency range.

Experimental curves showing the frequency dispersion for μ'_{eff} (red solid line) and for μ''_{eff} (blue solid line), for every specimen, can be found in Figures S1-S60.

3 | RESULTS AND DISCUSSION

Figure 1 depicts the frequency dispersion (real part – solid lines and imaginary part – dotted lines) for two specimens with the same chemical composition (that of the studied ferrite) but with different sintered microstructure. As shown in this figure, the real part of the magnetic complex permeability decreases with frequency (relaxation curve) while peaks in the imaginary part, highlighting the strong influence of this second with frequency dispersion. Figure 2 shows the scanning electron micrographs of polished and etched cross-sectional surfaces of both specimens of Figure 1, where, particularly, different average grain size can be observed. No precipitated phases can be identified at the grain boundaries (as the crystalline phases of zinc or copper found at certain sintering conditions in previous studies), suggesting that the chemical composition of the grains has remained constant throughout the sintering process.[44–46] Same evidence can be extended to all sixty specimens studied. The x-ray diffraction (XRD) pattern has also been verified to be the same for all 60 specimens.[47]

Equations (12) and (13) allow to determine the values of the magnetic permeability as a function of the microstructure (G and ϕ) and angular frequency. In order to use both equations to fit experimental frequency dispersion and to determine the characteristic material parameters, two additional considerations must be taken into account:

(i) b' shall be considered constant [40]:

$$b' = \alpha \tag{14}$$

(ii) b'' values, which were previously obtained by the authors for the four angular frequencies studied (10^6, 10^7, 10^8, and 10^9 Hz),[11] have now been empirically

TABLE 1 Processing conditions and sintered microstructural properties of the Cu-doped Ni-Zn-polycrystalline ferrite specimens

P (MPa)	T (°C)	t (min)	ϕ	$\varepsilon(\phi)$	G (μm)	ε(G) (μm)	S (G_{90}-G_{10}) (μm)	R^2 for μ'	R^2 for μ''
50	1100	5	0.832	0.005	3.4	0.2	4.0	0.9743	0.9761
		10	0.853	0.004	4.5	0.5	5.0	0.9861	0.9896
		20	0.876	0.003	5.6	0.2	6.3	0.9937	0.9945
		30	0.883	0.004	6.5	0.4	8.4	0.9959	0.9965
		45	0.896	0.002	7.6	0.5	8.5	0.9973	0.9981
		60	0.901	0.001	8.6	0.4	10.1	0.9987	0.9986
		120	0.912	0.001	11.1	1.0	13.1	0.9992	0.9996
		300	0.921	0.001	15.5	0.6	18.5	0.9995	0.9997
		900	0.928	0.002	19.4	0.8	23.7	0.9992	0.9987
		1800	0.930	0.001	20.5	2.0	26.3	0.9989	0.9976
75	1100	5	0.856	0.005	3.4	0.2	4.0	0.9807	0.9755
		10	0.878	0.003	4.6	0.5	5.4	0.9891	0.9897
		20	0.898	0.025	5.8	0.2	6.6	0.9948	0.9949
		30	0.906	0.001	6.9	0.4	8.7	0.9966	0.9972
		45	0.917	0.001	8.0	0.5	8.7	0.9979	0.9983
		60	0.918	0.001	9.1	0.4	10.9	0.9988	0.9989
		120	0.931	0.002	11.9	1.0	13.9	0.9996	0.9996
		300	0.938	0.001	15.9	0.6	18.8	0.9995	0.9994
		900	0.943	0.001	19.9	0.8	23.7	0.9993	0.9988
		1800	0.944	0.001	20.9	0.8	26.2	0.9988	0.9965
100	1100	5	0.867	0.007	3.5	0.1	4.1	0.9808	0.9762
		10	0.889	0.004	4.7	0.5	5.7	0.9890	0.9901
		20	0.908	0.002	6.1	0.6	7.2	0.9948	0.9955
		30	0.915	0.001	7.4	0.4	8.8	0.9968	0.9972
		45	0.926	0.001	8.4	0.9	11.1	0.9978	0.9980
		60	0.930	0.001	10.2	0.6	11.8	0.9987	0.9986
		120	0.938	0.001	12.6	0.6	15.4	0.9996	0.9997
		300	0.946	0.001	16.9	0.8	19.0	0.9995	0.9993
		900	0.951	0.002	20.2	0.6	24.2	0.9992	0.9983
		1800	0.952	0.001	21.1	5.0	27.2	0.9989	0.9979
150	1100	5	0.884	0.005	3.5	0.1	4.2	0.9818	0.9762
		10	0.904	0.003	4.8	0.5	5.7	0.9892	0.9902
		20	0.921	0.002	6.3	0.6	7.8	0.9956	0.9956
		30	0.929	0.002	7.4	0.4	8.5	0.9972	0.9971
		45	0.938	0.001	8.9	0.9	10.8	0.9978	0.9969
		60	0.941	0.001	10.2	0.6	10.5	0.9990	0.9988
		120	0.946	0.001	12.9	0.6	15.5	0.9996	0.9997
		300	0.955	0.001	16.9	0.8	19.6	0.9997	0.9996
		900	0.958	0.001	20.2	0.6	23.9	0.9992	0.9991
		1800	0.960	0.001	23.2	0.4	28.6	0.9988	0.9984
200	1100	5	0.893	0.004	3.5	0.2	4.3	0.9817	0.9750
		10	0.911	0.003	5.0	0.4	6.0	0.9886	0.9894
		20	0.928	0.001	6.5	0.5	8.4	0.9949	0.9946
		30	0.937	0.001	7.5	0.6	8.3	0.9969	0.9965
		45	0.943	0.001	9.0	0.5	10.5	0.9977	0.9968
		60	0.946	0.001	10.3	0.8	10.9	0.9990	0.9993
		120	0.954	0.001	13.5	0.2	15.8	0.9996	0.9997
		300	0.960	0.001	16.9	0.8	20.7	0.9996	0.9992
		900	0.961	0.002	20.2	0.7	23.1	0.9990	0.9991
		1800	0.963	0.001	22.7	1.0	29.0	0.9987	0.9986

(Continues)

TABLE 1 (Continued)

P (MPa)	T (°C)	t (min)	ϕ	$\varepsilon(\phi)$	G (μm)	ε(G) (μm)	S (G_{90}-G_{10}) (μm)	R^2 for μ'	R^2 for μ''
300	1100	5	0.896	0.004	3.6	0.2	4.3	0.9703	0.9658
		10	0.914	0.004	5.1	0.5	6.0	0.9829	0.9772
		20	0.933	0.001	6.7	0.2	8.7	0.9927	0.9917
		30	0.943	0.001	7.6	0.4	8.1	0.9963	0.9967
		45	0.950	0.001	9.2	0.5	10.5	0.9977	0.9977
		60	0.953	0.001	10.4	0.4	10.8	0.9992	0.9994
		120	0.957	0.001	13.7	1.0	16.0	0.9997	0.9994
		300	0.964	0.001	17.1	0.6	21.0	0.9995	0.9993
		900	0.964	0.001	20.3	0.8	23.0	0.9989	0.9990
		1800	0.967	0.001	22.0	0.9	26.2	0.9986	0.9987

Abbreviations: min, minutes; T, temperature; t, time.

TABLE 2 Values of the parameters estimated from Equations (16) and (17)

Parameter	Value	Units
K_S	600	–
ω_S	$7.79{\cdot}10^6$	Hz
K_{DW}	2950	–
ω_{DW}	$1.47{\cdot}10^8$	Hz
β	$1.93{\cdot}10^{10}$	Hz
α	3	μm^2

fitted to an exponential curve of the following equation:

$$b''(\omega) = 37 \cdot e^{-3{,}31\cdot 10^{-7}\cdot\omega} \tag{15}$$

Taking into account the last two conditions, Equations (12) and (13) become:

$$\mu'(\omega) = 1 + \left[\frac{K_S \cdot \omega_S}{\omega^2 + \omega_S^2}\right] \cdot \psi + \left[\frac{K_{DW} \cdot \omega_{DW}^2 \cdot \left(\omega_{DW}^2 - \omega^2\right)}{\left(\omega_{DW}^2 - \omega^2\right)^2 + \beta^2 \cdot \omega^2}\right] \cdot \left(\frac{G^2}{\alpha + G^2}\right) \cdot \psi \tag{16}$$

$$\mu''(\omega) = \left[\frac{K_S \cdot \omega \cdot \omega_S}{\omega^2 + \omega_S^2}\right] \cdot \psi + \left[\frac{K_{DW} \cdot \omega_{DW}^2 \cdot \beta \cdot \omega}{\left(\omega_{DW}^2 - \omega^2\right)^2 + \beta^2 \cdot \omega^2}\right] \cdot \left[\frac{G^2}{37 \cdot e^{-3{,}31\cdot 10^{-7}\cdot\omega} + G^2}\right] \cdot \psi \tag{17}$$

A nonlinear least-squares method has been used to fit experimental data (see Figures S1-S60) to Equations (16) and (17), allowing the estimation of constants K_S, K_{DW}, ω_S, ω_{DW}, α, and β by minimizing the sum of squared residuals. Table 2 depicts these estimated values, which can be introduced in Equations (16) and (17) yielding to the following:

$$\mu'(\omega) = 1 + \left[\frac{4.37 \cdot 10^9}{\omega^2 + 5.31 \cdot 10^{13}}\right] \cdot \psi + \left[\frac{6.37 \cdot 10^{19} \cdot \left(2.16 \cdot 10^{16} - \omega^2\right)}{\left(2.16 \cdot 10^{16} - \omega^2\right)^2 + 3.72 \cdot 10^{20} \cdot \omega^2}\right] \cdot \left(\frac{G^2}{3 + G^2}\right) \cdot \psi \tag{18}$$

$$\mu''(\omega) = \left[\frac{4.37 \cdot 10^9 \cdot \omega}{\omega^2 + 5.31 \cdot 10^{13}}\right] \cdot \psi + \left[\frac{1.23 \cdot 10^{30} \cdot \omega}{\left(2.16 \cdot 10^{16} - \omega^2\right)^2 + 3.72 \cdot 10^{20} \cdot \omega^2}\right] \cdot \left[\frac{G^2}{37 \cdot e^{-3{,}31\cdot 10^{-7}\cdot\omega} + G^2}\right] \cdot \psi \tag{19}$$

As an illustrative example, Figures 3 and 4 show the calculated complex permeability using Equations (18) and (19) for a specimen with an average grain size of 15.50 μm and a relative density of 0.92 (the same information can be seen together in Figure S7), where the solid black line stands for the estimated values, and red and blue circles stand for the experimental values of real and imaginary part, respectively. Figures S1-S60 show the same representation for all 60 specimens studied in the range of angular frequencies tested. As can be observed, the calculated values are in good agreement with experimental data, being slightly better for those specimens with higher relative density and average grain size, which, indeed, are

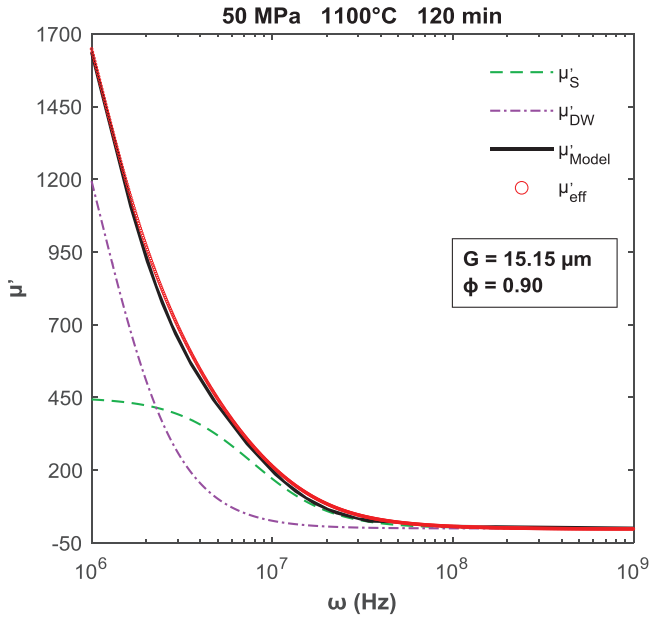

FIGURE 3 Experimental and calculated values using Equations (18) and (19) of complex magnetic permeability - real part and calculated values of spin rotation and domain-wall motion contributions

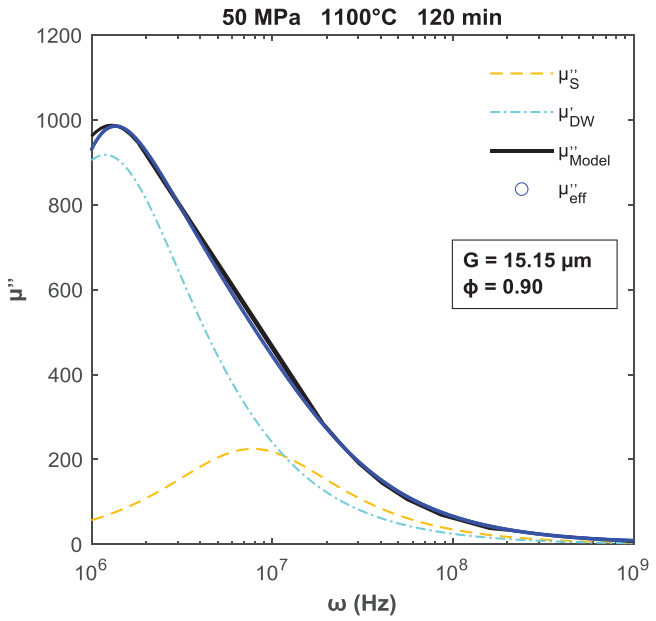

FIGURE 4 Experimental and calculated values using Equations (18) and (19) of complex magnetic permeability - imaginary part and calculated values of spin rotation and domain-wall motion contributions

the more interesting specimens from a technological point of view.

To quantify the good agreement, the complex magnetic permeability–real and imaginary part–can be calculated from Equations (18) and (19) for the 800 points that make up each experimental curve. The representation of the values of the real and imaginary parts of the complex magnetic permeability calculated versus the experimental ones gives straight lines with a slope of 1 that pass through the origin of coordinate. The squared correlation coefficients (R^2) are shown in Table 1. The R^2 values are very close to 1, except for specimens with relative density around 0.85. In any case, R^2 is greater than 0.97, which confirms the good agreement between experimental and calculated values in the entire range of tested frequencies.

The accurately fitting of both real and imaginary part of the complex magnetic permeability strengthens the concept of a relaxation curve for the real part and reinforces the idea of a curve that passes through a maximum for the imaginary part.

Furthermore, to consider the contribution of spin rotation and domain-wall motion mechanisms to complex magnetic permeability, Equations (18) and (19) can be separated in two terms as follows:

$$\mu'_S(\omega) = 1 + \left[\frac{4.37 \cdot 10^9}{\omega^2 + 5.31 \cdot 10^{13}}\right] \cdot \psi \tag{20}$$

$$\mu'_{DW}(\omega) = \left[\frac{6.37 \cdot 10^{19} \cdot \left(2.16 \cdot 10^{16} - \omega^2\right)}{\left(2.16 \cdot 10^{16} - \omega^2\right)^2 + 3.72 \cdot 10^{20} \cdot \omega^2}\right] \cdot \left(\frac{G^2}{3 + G^2}\right) \cdot \psi \tag{21}$$

$$\mu''_S(\omega) = \left[\frac{4.37 \cdot 10^9 \cdot \omega}{\omega^2 + 5.31 \cdot 10^{13}}\right] \cdot \psi \tag{22}$$

$$\mu''_{DW}(\omega) = \left[\frac{1.23 \cdot 10^{30} \cdot \omega}{\left(2.16 \cdot 10^{16} - \omega^2\right)^2 + 3.72 \cdot 10^{20} \cdot \omega^2}\right] \cdot \left[\frac{G^2}{37 \cdot e^{-3{,}31 \cdot 10^{-7} \cdot \omega} + G^2}\right] \cdot \psi \tag{23}$$

By way of example once again, Figures 3 and 4 (and Supplementary Fig. 1 to 60), show the contribution of every magnetizing mechanism (dot lines) to the complex magnetic permeability in the range of angular frequencies tested. Spin rotation contribution is higher than domain-wall contribution at low angular frequencies, as general rule. However, spin rotation contribution

decreases until reaching similar or even lower values than domain-wall motion contribution when increasing angular frequency.[4–7,11,16–18,21,24,48]

The values of fitting parameters shown in Table 2 are in good agreement with previous ones obtained by the authors for the same Cu-doped Ni-Zn ferrite [11] and with the values reported in literature for similar NiZn ferrites.[4,5,7,18,30] However, fitting values reported in literature are determined for a unique microstructure, and they can be distorted by the effect of relative density and grain size. It must be remarked again that the parameters shown in Table 2 are independent of angular frequency and, especially, of the microstructure. They are characteristic parameters of the material and valid for a wide range of average grain sizes and relative densities in the range of angular frequencies tested.

4 | CONCLUSIONS

The complex magnetic permeability (μ) of a polycrystalline Cu-doped Ni-Zn ferrite of chemical composition $Cu_{0.12}Ni_{0.23}Zn_{0.65}(Fe_2O_4)$ used as an electromagnetic wave absorber, has been quantitatively related to angular frequency (ω) of an AC magnetic field and, simultaneously, to the microstructure of the sintered specimens mainly characterized by their relative density (ϕ) and average grain size (G).

Literature gathers separately the influence of angular frequency (for a unique microstructure) or the influence of microstructure (at a fixed angular frequency) on the magnetic permeability. Here, a new mathematical model, expressed by Equations (16) and (17), has been developed to predict both real (μ') and imaginary (μ'') part of the complex magnetic permeability at a wide range of angular frequencies and microstructures. Both equations include a first term for the spin rotation mechanism and a second one for the domain-wall motion. In turn, first term is dependent on relative density whereas second term is dependent on relative density and on average grain size. This model allows to accurately reproduce the experimental values of μ' and μ'' to any angular frequency between 10^6 and 10^9 Hz and for a wide range of sintered microstructures.

The static susceptibility of the spin rotation (K_S) and domain-wall motion (K_{DW}) and the resonance frequency of the spin rotation (ω_S) and domain-wall motion (ω_{DW}) have been determined as intrinsic parameters of the $Cu_{0.12}Ni_{0.23}Zn_{0.65}(Fe_2O_4)$ ferrite, not dependent on frequency or microstructure.

The model also enables to display the evolution of magnetizing mechanism (spin rotation and domain-wall motion) with angular frequency and microstructure for both real (μ'_S, μ'_{DW}) and imaginary (μ''_S, μ''_{DW}) part of the complex magnetic permeability according to Equations (20) to (23). It has been observed that, at low angular frequencies, spin rotation contribution is higher than domain-wall: by increasing angular frequency, the first-one decreases until reaching similar or even lower values than the second-one.

In conclusion, the particularity of the model lies in the fact that it is possible to determine the magnetic permeability of a polycrystalline ferrite with a high degree of accuracy at any angular frequency (in the studied range) knowing the average grain size and the relative density.

ACKNOWLEDGMENTS

This study has been supported by Ministerio de Economía y Competitividad (Spain) (grant number: MAT2016−76320-R) and by Universitat Jaume I (Spain) (grant numbers: UJIB2017-48, UJIB2020-13, and POS-DOC/2020/04). Complex relative permeability determination was carried out at the central facilities (Servei Central d'Instrumentació Científica) of the Universitat Jaume I (Spain).

CONFLICT OF INTEREST

The authors declare that they have no known competing financial interests or personal relationships that could have appeared to influence the work reported in this paper.

ORCID

Carolina Clausell-Terol https://orcid.org/0000-0002-7781-4657

REFERENCES

1. Goldman A. Modern ferrite technology. 2nd ed. New York; London: Springer; 2006 https://doi.org/10.1017/CBO9781107415324.004
2. Barba A, Clausell C, Jarque JC, Nuño L. Magnetic complex permeability (imaginary part) dependence on the microstructure of a Cu-doped Ni–Zn-polycrystalline sintered ferrite. Ceram Int. 2020;46:14558–66. https://doi.org/10.1016/j.ceramint.2020.02.255
3. Guillaud C. The properties of manganese-zinc ferrites and the physical processes governing them. Inst Electr Eng. 1957;104:165–73. https://doi.org/10.1049/pi-b-1.1957.0023
4. Tsutaoka T. Frequency dispersion of complex permeability in Mn-Zn and Ni-Zn spinel ferrites and their composite materials. J Appl Phys. 2003;39:2789–96. https://doi.org/10.1063/1.1542651
5. Caltun OF, Spinu L, Stancu A, Thung LD, Zhou W. Study of the microstructure and of the permeability spectra of Ni-Zn-Cu ferrites. J Magn Magn Mater. 2002;242–245:160–2. https://doi.org/10.1016/S0304-8853(01)01187-8
6. Kawano K, Sakurai N, Kusumi S, Kishi H. Magnetic permeability and microstructure of the Bi,Si oxides-doped NiZnCu ferrite composite material. J Magn Magn Mater. 2006;297:26–32. https://doi.org/10.1016/j.jmmm.2005.01.033

7. Su H, Zhang H, Tang X, Jing Y, Zhong Z. Complex permeability and permittivity spectra of polycrystalline Ni-Zn ferrite samples with different microstructures. J Alloys Compd. 2009;481:841–4. https://doi.org/10.1016/j.jallcom.2009.03.133
8. Kawano K, Hachiya M, Iijima Y, Sato N, Mizuno Y. The grain size effect on the magnetic properties in NiZn ferrite and the quality factor of the inductor. J Magn Magn Mater. 2009;32:2488–93. https://doi.org/10.1016/j.jmmm.2009.03.015
9. Jahanbin T, Hashim M, Amin Mantori K. Comparative studies on the structure and electromagnetic properties of Ni-Zn ferrites prepared via co-precipitation and conventional ceramic processing routes. J Magn Magn Mater. 2010;322(18):2684–9. https://doi.org/10.1016/j.jmmm.2010.04.008
10. Costa ACFM, Tortella E, Morelli MR, Kiminami RHGA. Synthesis, microstructure and magnetic properties of Ni-Zn ferrites. J Magn Magn Mater. 2003;256(1–3):174–182. https://doi.org/10.1016/S0304-8853(02)00449-3
11. Barba-Juan A, Vicente N, Mormeneo-Segarra A, Clausell-Terol C. Influence of microstructure and magnetizing mechanisms on magnetic complex permeability (imaginary part) of a Cu-doped Ni–Zn polycrystalline ferrite. Ceram Int. 2021;47:29504-29508. https://doi.org/10.1016/j.ceramint.2021.07.119
12. Hamilton N. The small-signal frequency response of ferrites. High Freq Electron. 2011;10:36–52.
13. Nakamura T. Study on high-frequency permeability in ferrite ceramics and ferrite composite materials. Hiroshima, Japan: Hiroshima University; 1996.
14. Ponomarenko N. Study of frequency and microstructure dependencies of magnetic losses of ferrite materials and components. Riga, Latvia: Riga Technical University; 2014
15. Guyot M, Merceron T, Cagan V, Messekher A. Mobility and/or damping of the domain wall. Phys status solidi. 1988;106:595–612. https://doi.org/10.1002/pssa.2211060232
16. Nakamura T. Low-temperature sintering of Ni-Zn-Cu ferrite and its permeability spectra. J Magn Magn Mater. 1997;168(96):285–91. https://doi.org/10.1016/S0304-8853(96)00709-3
17. Fano WG, Boggi S, Razzitte AC. Causality study and numerical response of the magnetic permeability as a function of the frequency of ferrites using Kramers-Kronig relations. Phys B Condens Matter. 2008;403:526–30. https://doi.org/10.1016/j.physb.2007.08.218
18. Tsutaoka T, Ueshima M, Tokunaga T, Nakamura T, Hatakeyama K. Frequency dispersion and temperature variation of complex permeability of Ni-Zn ferrite composite materials. J Appl Phys. 1995;78:3983–91. https://doi.org/10.1063/1.359919
19. Nakamura T, Tsutaoka T, Hatakeyama K. Frequency dispersion of permeability in ferrite composite materiales. J Magn Magn Mater. 1994;138(3):319–28. https://doi.org/10.1016/0304-8853(94)90054-X
20. Yan S, Liu S, He L, He J, Huang S, Deng L. Investigation on microstructure and magnetic properties in V2O5 doped NiCuZn ferrite. Mater Res Express. 2019;6(7):076111. https://doi.org/10.1088/2053-1591/ab1782
21. Boggi S, Fano WG. Numerical response and causality study of the magnetic permeability-frequency function of NiZn ferrites using genetic algorithm. J Magn Magn Mater. 2020;500:166305. https://doi.org/10.1016/j.jmmm.2019.166305
22. Razzitte AC, Fano WG, Jacobo SE. Electrical permittivity of Ni and NiZn ferrite-polymer composites. Phys B Condens Matter. 2004;354:228–231. https://doi.org/10.1016/j.physb.2004.09.054
23. Jankovskis J. Complex permeability of ferrites correlated with their microstructure. Adv Sci Technol. 2006;45:2560–5. https://doi.org/10.4028/www.scientific.net/ast.45.2560
24. Stergiou CA, Zaspalis V. Analysis of the complex permeability of NiCuZn ferrites up to 1 GHz with regard to Cu content and sintering temperature. Ceram Int. 2014;40:357–66. https://doi.org/10.1016/j.ceramint.2013.06.010
25. Johnson MT, Visser EG. A coherent model for the complex permeability in polycrystalline ferrites. IEEE Trans Magn. 1990;26:1987–9. https://doi.org/10.1109/20.104592
26. Van Der Zaag PJ, Ruigrok JJM, Noordermeer A. The initial permeability of polycrystalline MnZn ferrites: the influence of domain and microstructure. J Appl Phys. 1993;74:4085–95. https://doi.org/10.1063/1.354454
27. Gieraltowski J. Initial susceptibility frequency spectra and distribution of the grain sizes in Ni-Zn and YIG polycrystalline ferrites. J Magn Magn Mater. 1989;81:103–6. https://doi.org/10.1016/0304-8853(89)90235-7
28. Syazwan MM, Hapishah AN, Azis RS, Abbas Z, Hamidon MN. Grain growth effects on magnetic properties of Ni0.6Zn0.4Fe2O4material prepared using mechanically alloyed nanoparticles. Results Phys. 2018;9:842–50. https://doi.org/10.1016/j.rinp.2018.03.054
29. Kong LB, Li ZW, Lin GQ, Gan YB. Electrical and magnetic properties of magnesium ferrite ceramics doped with Bi2O3. Acta Mater. 2007;55:6561–72. https://doi.org/10.1016/j.actamat.2007.08.011
30. Manjurul Haque M, Huq M, Hakim MA. Influence of CuO and sintering temperature on the microstructure and magnetic properties of Mg- Cu- Zn ferrites. J Magn Magn Mater. 2008;320:2792–9. https://doi.org/10.1016/j.jmmm.2008.06.017
31. Mirzaee O, Shafyei A, Golozar MA, Shokrollahi H. Influence of MoO3 and V2O5 co-doping on the magnetic properties and microstructure of a Ni-Zn ferrite. J Alloys Compd. 2008;461:312–315. https://doi.org/10.1016/j.jallcom.2007.06.120
32. Ismail I, Hashim M. Sintering temperature dependence of evolving morphologies and magnetic properties of Ni0.5Zn0.5Fe2O4 synthesized via mechanical alloying. J Supercond Nov Magn. 2012;25:1551–61. https://doi.org/10.1007/s10948-012-1468-6
33. Ismail I, Hashim M, Amin Matori K, Alias R, Hassan J. Dependence of magnetic properties and microstructure of mechanically alloyed Ni 0.5Zn 0.5Fe 2O 4 on soaking time. J Magn Magn Mater. 2012;324:2463–70. https://doi.org/10.1016/j.jmmm.2012.03.012
34. Kang S-JL. Grain growth and densification in porous materials. Sintering: densification, grain growth and microstructure. Burlington: Elsevier; 2005. https://doi.org/10.1016/b978-075066385-4/50011-x
35. Globus A. Some physical considerations about the domain wall size theory of magnetization mechanisms. J Phys Colloq. 1977;38:C1.1–15. https://doi.org/10.1051/jphyscol:1977101
36. Globus A, Duplex P, Guyot M. Determination of initial magnetization curve from crystallites size and effective anisotropy field. IEEE Trans Magn. 1971;7(3):617–22. https://doi.org/10.1109/TMAG.1971.1067200

37. Postupolski T, Wisniewska A. Size dependence of the thermally and magnetically induced wall pinning in a Ni-Zn ferrite. J Phys Colloq. 1977;38:C1.31–4. https://doi.org/10.1051/jphyscol:1977105
38. Rikukawa H. Relationship between microstructures and magnetic properties of ferrites containing closed pores. IEEE Trans Magn. 1982;18(6):1535–7. https://doi.org/10.1109/TMAG.1982.1062065
39. Hanuszkiewicz J, Holz D, Eleftheriou E, Zaspalis V. Materials processing issues influencing the frequency stability of the initial magnetic permeability of MnZn ferrites. J Appl Phys. 2008;103:103907–110. https://doi.org/10.1063/1.2932062
40. Pankert J. Influence of grain boundaries on complex permeability in MnZn ferrites. J Magn Magn Mater. 1994;138:45–51. https://doi.org/10.1016/0304-8853(94)90397-2
41. German RM. Sintering theory and practice. 1st ed. New York: John Wiley & Sons, Inc.; 1996
42. Clausell C, Barba A, Nuño L, Jarque JC. Electromagnetic properties of ferrite tile absorber as a function of compaction pressure. Ceram Int. 2016;42(15):17303–9. https://doi.org/10.1016/j.ceramint.2016.08.026
43. Clausell C, Barba A, Nuño L, Jarque JC. Effect of average grain size and sintered relative density on the imaginary part – μ'' of the complex magnetic permeability of (Cu0.12Ni0.23Zn0.65)Fe2O4 system. Ceram Int. 2016;42(3):4256–61. https://doi.org/10.1016/j.ceramint.2015.11.101
44. Barba A, Clausell C, Jarque JC, Monzó M. ZnO and CuO crystal precipitation in sintering Cu-doped Ni-Zn ferrites. I. Influence of dry relative density and cooling rate. J Eur Ceram Soc. 2011;31(12):2119–28. https://doi.org/10.1016/j.jeurceramsoc.2011.05.007
45. Low KO, Sale FR. Electromagnetic properties of gel-derived NiCuZn ferrites. J Magn Magn Mater. 2002;246:30–5. https://doi.org/10.1016/S0304-8853(01)01390-7
46. Hsiang HI, Kuo WC, Hsi CS. Sintering and cooling atmosphere effects on the microstructure, magnetic properties and DC superposition behavior of NiCuZn ferrites. J Eur Ceram Soc. 2017;37:2123–8. https://doi.org/10.1016/j.jeurceramsoc.2017.01.025
47. Vicente N, Mormeneo-segarra A, Clausell-terol C, Barba-Juan A. New model to tune the dielectric properties of dense and half-dense sintered polycrystalline cu-doped Ni – Zn ferrite. J Eur Ceram Soc. 2021. https://doi.org/10.1016/j.jeurceramsoc.2021.11.026
48. Mahmud ST, Akther Hossain AKM, Abdul Hakim AKM, Seki M, Kawai T, Tabata H. Influence of microstructure on the complex permeability of spinel type Ni-Zn ferrite. J Magn Magn Mater. 2006;305(1):269–74. https://doi.org/10.1016/j.jmmm.2006.01.012

SUPPORTING INFORMATION

Additional supporting information may be found in the online version of the article at the publisher's website.

How to cite this article: Barba-Juan A., Mormeneo-Segarra A, Vicente N, Jarque JC, Clausell-Terol C. Frequency dispersion model of the complex permeability of soft ferrites in the microwave frequency range. J Am Ceram Soc. 2022;105:2725–2734. https://doi.org/10.1111/jace.18267